



Bulletin of the Mineral Research and Exploration

<http://bulletin.mta.gov.tr>



Time-lapse ground penetrating radar (GPR) imaging of used engine oil contamination

Hafız MOHAMMED NAZİFİ^{a*}, Ertan PEKŞEN^b, Ertuğrul GÜRBÜZ^a and Levent GÜLEN^a

^a Sakarya University, Department of Geophysical Engineering, Sakarya University, Sakarya, Türkiye

^b Kocaeli University, Department of Geophysical Engineering, Kocaeli, Türkiye

Research Article

Keywords:

Ground Penetrating Radar (GPR), Used Engine Oil (UEO), Contamination, Light Non-Aqueous Phase Liquid (LNAPL), Environmental Geophysics.

ABSTRACT

Time-Lapse Ground Penetrating Radar (GPR) was employed to study used engine oil (UEO) contamination of sandy environment in laboratory setting. GPR is a near-surface geophysical method that uses electromagnetic field to provide image of the dielectric properties of earth materials to detect structures and changes in material properties within the subsurface. This research aimed to detect, monitor and map the migration of UEO contaminant in sand. The results of this study revealed that the migration of the UEO contamination in homogeneously laid sand is non-uniform. UEO plumes were identified as high amplitude signals with enhanced reflectivity. There was a progressive decrease in GPR signal amplitudes (reflection reduction) within the contaminated area of the tank with time. This decrease of GPR signal amplitudes was interpreted as caused by the evaporation of some portion of the UEO in the vadose zone as a result of temperature increase in time and also due to the occurrence of UEO biodegradation. The time-lapse GPR proved to be an effective technique for detecting, monitoring, and mapping UEO migration within sand tank in laboratory setting.

Received Date: 29.10.2022

Accepted Date: 12.04.2023

1. Introduction

The modern world suffers from environment problems such as soil and groundwater contamination as a result of anthropogenic activities. Improper disposal of UEO cause serious environmental issue. The UEO is used as an auxiliary fuel in industrial steam boilers, domestic oil burners, utility steam boilers, waste disposal incinerators and rotary cement kilns (ATSDR, 1997). It is also used as a component in asphalt. UEO is re-refined to make lubricating oil. Maceiras et al. (2017) stated that 45 million tons (estimated) of UEO are generated each year in the world and about only 18 million tons of this oil collected and disposed properly. El-Fadel and Khoury (2001), estimated that in 1995 less than 45% of UEO were being collected world-wide and about 55%

of UEO were either misused or discarded into the environment by the end user.

The health risks and their effects on livestock caused by UEO contaminations of soil and water bodies include convulsions, muscle twitching, neurological disorders, blindness, hyperirritability and depression. It also includes development of liver or kidney disease, possible damage to the bone marrow, increase risk of cancer, complete impairment of body functions and eventually death in livestock (Propst et al., 1999; Abioye et al., 2012; Nolin et al., 1990; El-Fadel and Khoury, 2001; Osweiler et al., 1973; Sas, 1989; ATSDR, 1997). Through food chain toxins accumulate in plants and animals and they could move up the food chain affecting the health of human beings.

Citation Info: Nazifi, H. M., Pekşen, E., Gürbüz, E., Gülen, L. 2024. Time-lapse ground penetrating radar (GPR) imaging of used engine oil contamination. Bulletin of the Mineral Research and Exploration 173, 175-188. <https://doi.org/10.19111/bulletinofmre.1282076>

*Corresponding author: Hafız Mohammed NAZİFİ, mohammednazifi@gmail.com

UEO is classified as Light Nonaqueous Phase Liquids (LNAPLs). LNAPLs are organic liquids that are lighter than water. Other examples of LNAPLs include gasoline, diesel, and jet fuel. LNAPLs tend to accumulate above and marginally below the water table. Disparities in the chemical and physical characteristics of water and LNAPL result in the formation of a physical interface between the liquids which impedes the mixture of the two fluids.

Investigation, management and remediation of LNAPL-affected sites are challenging due to their complexity (USEPA, 1993; Charbeneau et al., 1995; USEPA, 1996; Tomlinson et al., 2017; Ebrahimi et al., 2019; Boumaiza et al., 2022). Despite these challenges, there are many reports of successes in subsurface LNAPL investigation and detection. Methods of detecting the extent of contaminations, the migration patterns, and the evolution of LNAPL contaminated sites are broadly classified under two categories. These are the discrete point sampling of fluids and soil using wells or multi-level piezometers and the indirect measurement through surface or borehole geophysical techniques. Geophysical techniques offer opportunities for non-intrusive investigation of LNAPL contaminated sites.

Direct and indirect detection of LNAPL is possible with different geophysical methods such as resistivity, Induced Polarization, Electromagnetic Induction, GPR and Magnetic Susceptibility and others. This detection depends on the type and quantity of LNAPL, the earth material (such as clay contents), aqueous phase distribution and ionic strength (Monier-Williams, 1995). In general, electrical conductivity, and to a lesser extent GPR, can directly detect the presence of organic contaminants by measuring changes in soil conductivity caused by chemical compounds. The ability of geophysical methods to detect, characterize, and map organic pollutants at contaminated sites depends on the depth of the contamination. Smaller concentrations of pollutants could be detected using geophysical methods (USEPA, 2000; Arato et al., 2014; Ameen et al., 2014).

GPR has proven to be successful in mapping LNAPL and it has been ranked second after electrical methods for its ability to detect organic contaminants

(Atekwana and Atekwana, 2010). Fresh contaminated sites produced enhanced GPR signal amplitude and clean GPR reflection while 'aged' contaminations are characterized by high conductivity or GPR reflection signal reduction below conductive zones, usually at the top of aquifers. Another reason for the decrease in reflection zone or amplitude attenuation zone is increase in vapor pressure from volatile components in LNAPLs (Olhoeft, 1992; Douglas et al., 1992; Daniels et al., 1995; Grumman and Daniels, 1995; Maxwell and Schmock, 1995; Bermejo et al., 1997; Kim et al., 2000; Atekwana et al., 2002; Werkema et al., 2003).

Among site conditions which have been reported as favourable for detecting and monitoring LNAPLs using GPR include thick pools of contaminant, clay free, granular soils, diminishing capillary fringe thicknesses in more granular materials, shallow exploration depths, and homogeneity within the near-surface region (Olhoeft, 1986; Redman et al., 1994; Barber and Morey, 1994; Grumman and Daniels, 1995). The subsurface migration trends of LNAPL contaminants are due to a few factors that include subsurface geology and geological structures. According to Mineo et al. (2022), the fracturing of the rock mass and the presence of subsurface structures, probably of tectonic origin, are responsible for the contamination plume taking a preferential path under the dynamic conditions caused by anthropic activities. This supports the need for subsurface geology and geological structural knowledge in monitoring contaminant migrations. Azimi et al. (2020), who studied the movement of LNAPL into monitoring wells, stated that monitoring LNAPL migrations exposed to fluctuations in groundwater levels is a complex phenomenon. They point out that to understand the subsurface distribution of LNAPL, factors such as aquifer grain sizes and LNAPL properties must be considered.

According to Olhoeft (1992), most hydrocarbons are LNAPLs with low relative dielectric permittivity and higher vapor pressure. These LNAPLs can be delineated by GPR, both directly as a reflection from the dielectric contrast of a thick layer or due to a change in the water table reflection (generally higher reflectivity) from flattening or sharpening of the capillary fringe. The reflections from LNAPLs

in the near surface are a function of the permittivity contrast between the LNAPLs and the host material (Daniels et al., 1995). Cassidy (2007) stated that it is common to find a range of GPR responses at any given LNAPL contamination site with shadow zones being co-incident with 'bright spot' reflections and signal reduction varying significantly over the site. The findings of Cassidy (2007) show that highest signal attenuation is associated with either mixed phase, or a smeared zone where biodegraded LNAPLs co-exist with contaminated pore and groundwater. Bertolla et al. (2014), reported a study in which an experiment in controlled condition was carried out to test the effectiveness of the use of GPR to monitor oil spill contamination. Their results show that GPR is not effective in monitoring LNAPL plume in an unsaturated (dry) sand, but effective in saturated (wet) sand. They concluded that the ability to detect the contamination plume was due to the higher contrast between the electromagnetic properties of water-saturated sand and the oil LNAPL floating on the groundwater level. They suggested the acquisition of GPR data should be carried out shortly after a period of rainfall.

Although UEO is a common contaminant, investigation of the detection, mapping, and monitoring of UEO contaminated soils and aquifers have been overlooked, neglected so far. Currently, Nazifi et al. (2022) and Lago et al. (2009) are the only available published works that used geophysical methods to map and characterize a UEO contamination. Nazifi et al. (2022) used electrical resistivity tomography (ERT) method in monitoring the evolution of UEO contamination, while Lago et al. (2009) used GPR and ERT in mapping matured UEO disposal site. Their results revealed that, the UEO beneath the disposal site has undergone microbial degradation and their radargrams were characterized by high conductivity zone or GPR reflection attenuation below conductive zones. In this paper, we report on a 26 week long investigation of UEO contamination within a specially designed experiment tank in laboratory setting using time-lapse GPR. The objectives of the study were to detect UEO contamination within a sandy environment, to monitor and map the migration of the contaminant using time-lapse GPR.

2. Materials and Method

2.1. Contaminant

UEO was used to contaminate the setup. New engine oil and UEO are classified as LNAPLs. LNAPLs are hydrocarbons that are less dense than water and immiscible in water. LNAPLs are the most common organic contaminants that are found in the subsurface that contaminate soil and groundwater (Tomlinson et al., 2017; Newell, 1995). UEO is a mixture of high and low (C15-C50) molecular weight aromatic and aliphatic hydrocarbons, lubrication additives, metals, and various organic and inorganic compounds (ATSDR, 1997). The chemical composition of UEO varies widely and depends on the additives added to the fuel. There are generally four types of the engine oil which are full synthetic oil, synthetic blend or semi-synthetic oil, mineral or conventional oil and lastly high mileage oil.

Carey (1998) reported that the dielectric constant of motor oils at room temperature ranges between 2.1 to 2.8. Kardos and Pietrikova (2016) reported that the dielectric constant of new and used motor oils ranges between 2.1 to 2.4 depending on the temperature. The dielectric constant also depends on the viscosity of the oil, the paraffinic or naphthenic content and the additive package. The viscosity of motor oil depends on temperature, and it decreases with increase in temperature (Kardos and Pietrikova, 2016).

The UEO contaminant used in this experiment is a mixture of several used engine oils. It contains some elements such as Calcium, Zinc, Phosphorus etc. The specific gravity of the oil at 15°C is 877.9 kg/m³ and its kinematic viscosity at 40°C is 78.03 mm²/s. For further information on the chemical and physical properties of UEO see Table 1.

2.2. Experimental Setup

The experiment was carried out in a specially designed plexiglass tank. The tank has three chambers (Figure 1). The first and the third chambers have dimensions of 10 cm x 60 cm x 50 cm, and they are for water inlet and water outlet, respectively. The second (middle) chamber has the dimensions of 270 cm x 60 cm x 50 cm and it is filled with sand.

Table 1- Results of physical and chemical analysis of the UEO used in the experiment.

Parameters Measured	Method Applied	Results	Units
Metals			
Iron	IP 501	59	mg/kg
Nickel	IP 501	4.2	mg/kg
Vanadium	IP 501	<1	mg/kg
Aluminium	IP 501	14	mg/kg
Calcium	IP 501	2424	mg/kg
Zinc	IP 501	1170	mg/kg
Phosphorus	IP 501	951	mg/kg
Silica	IP 501	11	mg/kg
Sodium	IP 501	15	mg/kg
Carbon Residue Percentage Weight (Micro Method)	TS EN ISO 10370	2.27	(m/m) %
Water Content Percentage Weight	TS EN 1428	0.1	(v/v) %
Total Acidity	ASTN D 664	4.46	mgKOH/g
API, gravity (60F)	TS 1013 EN ISO 3697	29.6	API
Specific gravity at 15.0 °C		877.9	kg/m ³
Kinematic Viscosity at 40.0 °C	TS EN ISO 3104	78.03	mm ² /s

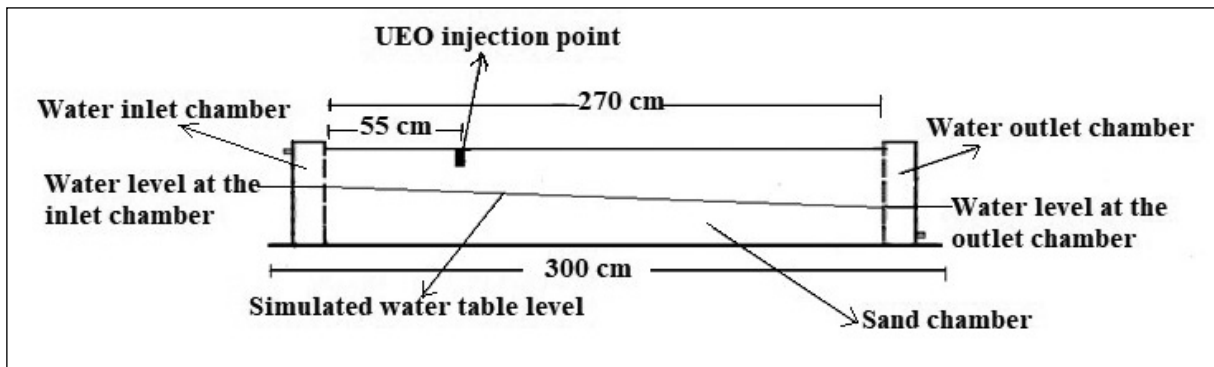


Figure 1- Sideway view (cross section) of the plexiglass tank used for the experiment.

The tank (sand chamber) was filled with a clean sand (Figure 2) obtained from the flood plain of the Sakarya river. The sand was modelled into saturated and unsaturated zone with the depth of the sand model set approximately at 45 cm from the bottom of the tank. Tap water was fed to flow through the tank. The water levels were kept at constant height of 25 cm at the inlet chamber and 15 cm at the outlet chamber, respectively.

Based on sieve analysis results, the sand consists of 1.06% of very fine sand particles, 72.05% fine and medium sand particles and 26.90% gravel. The sand was interpreted as a well sorted, clean, uniform sand with small amount of gravel.



Figure 2- Image of the plexiglass tank showing the three chambers of the tank and the profile lines (yellow lines).

The setup was first contaminated with 1.5 litres of UEO through a pit at a depth of 15 cm. But it was realized that the contaminant was not enough to migrate to the outlet end of the tank. Hence one week after the initial contamination, an additional 2.5 litres of UEO were injected through the same pit making the total volume of UEO contaminant 4.0 litres.

2.3. GPR Data Acquisition and Processing

GPR is a geophysical method that uses the transmission and reflection of high frequency (10 MHz to 2 GHz) EM waves within the near sub-surface. GPR signal depends on the properties of the earth such as the dielectric permittivity ϵ , the electrical conductivity σ , and the magnetic permeability μ (Knight, 2001). Further information on the fundamental principles of GPR can be found in publications by Daniels et al. (1988), Davis and Annan (1989); Knight (2001).

In our experiments GPR survey was conducted using the Zond – 12e GPR advanced (Radar System Inc.) system. Five sets of GPR data were collected and each data set consisted of eight profiles (for locations of the profiles see figure 2) making total of 40 GPR profiles. These add up to about 92 m of GPR profile data. The data were acquired in groups of eight profiles with 5 cm spacing between each profile. Figure 3 shows a photo taken during data acquisition. The data were acquired before (26.02.2020), one hour after (26.02.2020), two weeks after (04.03.2020), four weeks after (26.03.2020), and twenty-six weeks after (19.08.2020) the initial contamination.

The data were acquired with a shielded 2 GHz Zond antenna and the acquisition parameters were 1024 sample/trace and a scan rate of 40. The antenna was placed on a wooden rail during the data acquisition as seen in Figure 3. The wooden rail (Figure 3) helped in obtaining good reproducibility of the data (Bertolla et al., 2014).

Data were recorded in time window range between 0 and 1.88 m which is equivalent to 0 and 50 ns (nanoseconds), although some measurements were a bit little less than the 1.88 m. Data processing was carried out to improve signal to noise ratio and enhanced visualization. Data acquisition and post-processing were done using Prism 2 software (Radar

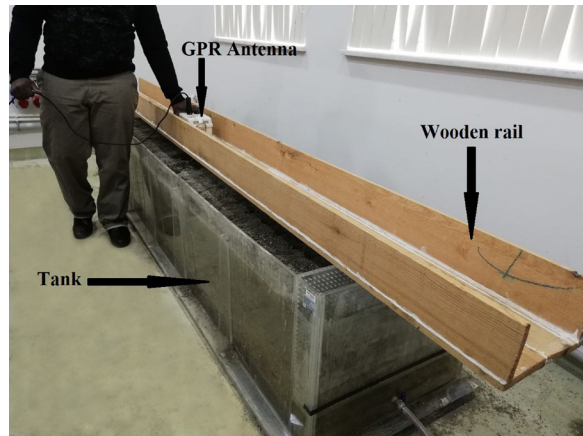


Figure 3- Image showing the plexiglass tank, the wooden rail and the GPR antenna during data acquisition.

System Inc.). The first step of the data processing was the subtraction of the data set obtained before oil contamination (this data is referred to as the background data) from all the data sets obtained after the contamination. The radar data processing included zero-time, background removal, Horizontal Low-Pass (LP) filter, move-out correction, migration [Stolt (F-K) method] and automatic gain control. Zero-time was applied to remove the effect of the wooden rail and the air between the wooden rail and the surface of the sand. Background removal was applied to efficiently suppress the background of the radargram. Horizontal LP filter was applied for the fast signal variable suppression. Move-out correction restores a profile to a pattern as if the signal radiated and recessed in a point located in the middle of the antenna. Lastly, migration is for the reconstruction of the original shape of underground interfaces and local objects by its radiolocation profile. The Stolt (F-K) method of migration provided by the Prism 2 software was used in performing migration. The hyperbola technique was used in determining the permittivity of contaminants within the experimental tank. From the hyperbola technique, the permittivity of the contaminated section of the radargram is given as 2.07. The velocity of signal through the contaminated section is given as 20.16 cm/ns. The possible surrounding medium of the hyperbola that was suggested by the software to consist of snow, ice, frozen oil and oil products. The oil product suggested by the software was due to the 2.07 permittivity is a good prediction, since the soil was contaminated with UEO. The obtained permittivity

value was used in the migration step. Automatic gain control was applied within the width of the window for each separate trace. It was used for levelling all signals in a trace. It makes the signals more visible.

Prism 2 program was used for aligning 2D profiles and converting them into 3D radargrams. Five 3D radargrams were created from the five sets of eight GPR profiles. The Easy Prism software (Radar Systems Inc.) was used for the 3D GPR visualization.

3. Conclusion and Discussion

2D Time-lapse vertical view of GPR radargrams from profile 5 (Figure 4 - XZ plane), 1D Time-lapse horizontal signal amplitude graphs at depth 15 cm (Figure 5), 1D Time-lapse vertical signal amplitude and attenuation graphs at a distance of 50 cm (Figure 6) and 3D cross sectional radargrams (Figure 7) were selected and presented in this paper. The radargrams as shown in Figures 4, 5, 6 and 7 were labelled a, b, c, d and e corresponding to the background, 1 hour, 2 weeks, 4 weeks, and 26 weeks after the initial contamination, respectively.

From both Figure 4 and Figure 7, one set of horizontal reflectors can be seen and they were indicated by yellow lines labelled F1 – F2 in Figure 4. The set of horizontal reflectors correspond to the simulated groundwater level are between about 24 cm to 46 cm. The reflector divides the radargrams into two parts, the upper unsaturated and the lower saturated parts. The strong reflectors are caused primarily by the sharp change in the permittivity in the transition from the unsaturated sand to the saturated sands. The UEO as LNAPLs might be displaced by water from the transition zone above the capillary fringes and therefore making a sharp interface at the top of the water saturated zone (de Castro and Branco, 2003). This might be the reason for the elevation of horizontal reflectors in Figure 4c and 4d. It was observed that the results (Figure 4b and 7b) obtained one hour after initial contamination showed a slight distortion of the groundwater level between points 0.13-1.0 m on the distance axis. The distortion of the groundwater was much pronounced after additional contamination of 2.5 litres, 2 weeks after the initial contamination (Figure 4c and 7c). The oil might have migrated both

vertically and horizontally, this is because of the anomalies revealed in both vertical and horizontal layers of Figures 7c and 7d. It can also be seen that there were afterwards, the groundwater level reflector was not much distorted compared to the background. The plume resulting from the initial contamination of the UEO could be seen on Figure 4b between 0 – 17 cm on the depth axis and between 0.13-0.88m on the distance axis. The anomalies in Figures 4c–d are much pronounced than that in Figure 4b. This is understandable, because the plume corresponding to the radargrams in Figures 4c–d is more voluminous than that in Figure 4b.

The horizontal layer shown in Figure 7 on the 3D time lapse radargrams is located at a depth of 25 cm. This was 10 cm downward of the contamination pit which was 15 cm from the surface of the tank. In reference to the background radargram (Figure 7a), we can see that there was a small anomaly in Figure 7b (1 hour after initial contamination). The anomaly is more obvious than in Figure 7c which is the results of 2 weeks after initial contamination of 1.5 litres of UEO and a week after additional contamination of 2.5 litres. The UEO migrated further downwards and horizontally and was recorded on both horizontal and vertical section of Figure 7d. The anomalies in both Figures 5e and 7e are attributed to residual UEO plume which has dielectric contrast compared to dry sand. The data of the results in Figures a-d were collected in late winter and early spring (between February and March) when the temperature relatively cold and the vadose zone is much moist. But the in Figure 7 e were collected in summer (August) when the temperature is much higher compared to winter and spring. The high temperature might have increased the evaporation of the upper vadose zone making the UEO residue to be solidified and the sand to be dry compared to the results in Figures 7a-d.

The time-lapse 3D radargrams (Figure 7) clearly show both vertical and lateral migration of UEO. The 3D radargrams are consistent with the 2D radargrams. Both the 2D and 3D results indicate that UEO initially migrated vertically (predominantly) and then horizontally. In other words, first the contaminant percolated down and then lateral migration became dominant.

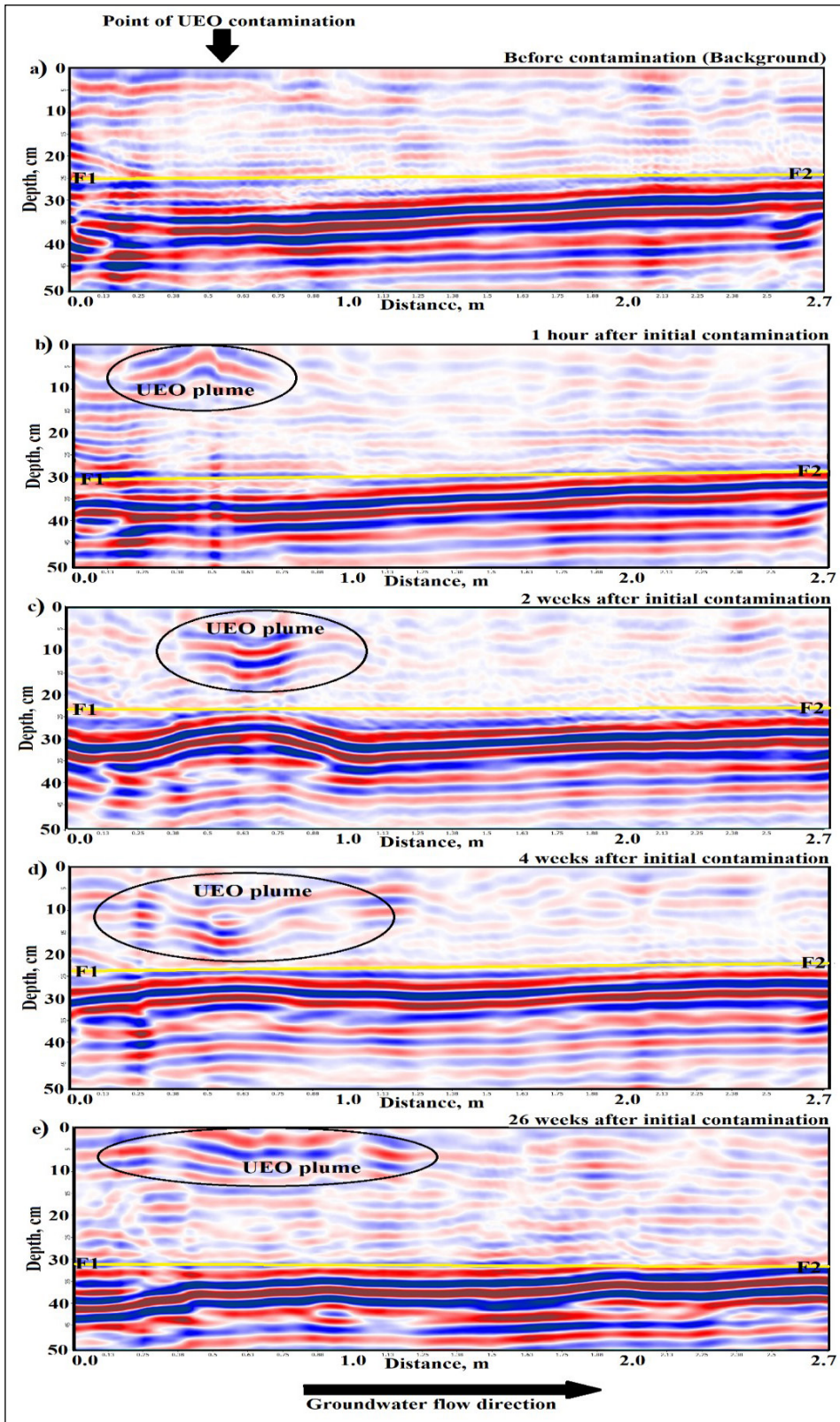


Figure 4 -2D Time-lapse vertical view of GPR radargrams from profile 5 (XZ plane). The yellow line labelled F1-F2 represents the boundaries between unsaturated and saturated sand, black circles indicate the extensions of the oil plume, a), b), c), d) and e) are the radargrams from data before contamination, one hour, 2 weeks, 4 weeks, and 26 weeks after initial contamination, respectively.

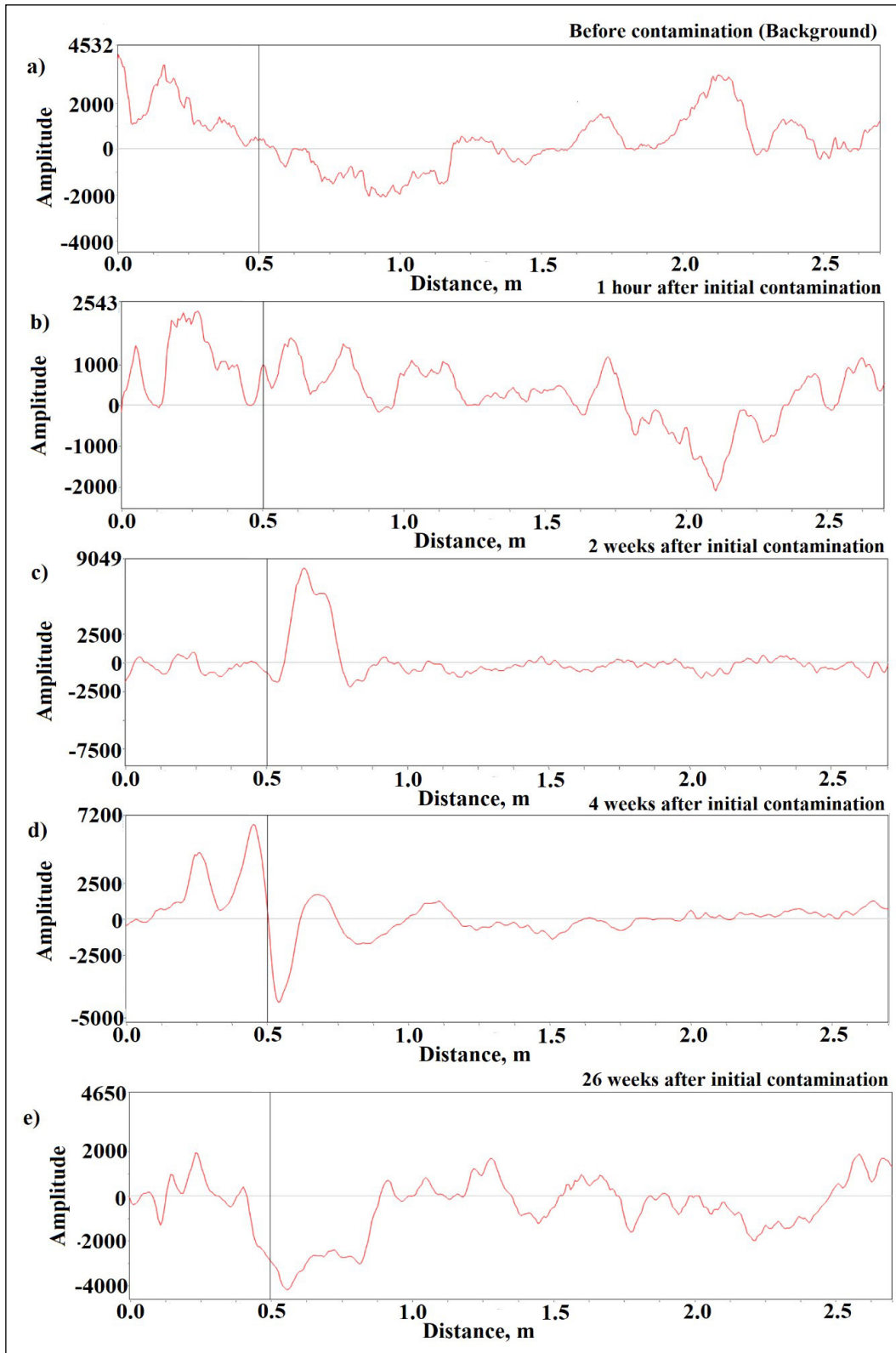


Figure 5- 1D Time-lapse horizontal signal amplitude graphs at depth 15 cm. a), b), c), d) and e) are the radargrams from data before contamination, one hour, 2 weeks, 4 weeks, and 26 weeks after initial contamination, respectively.

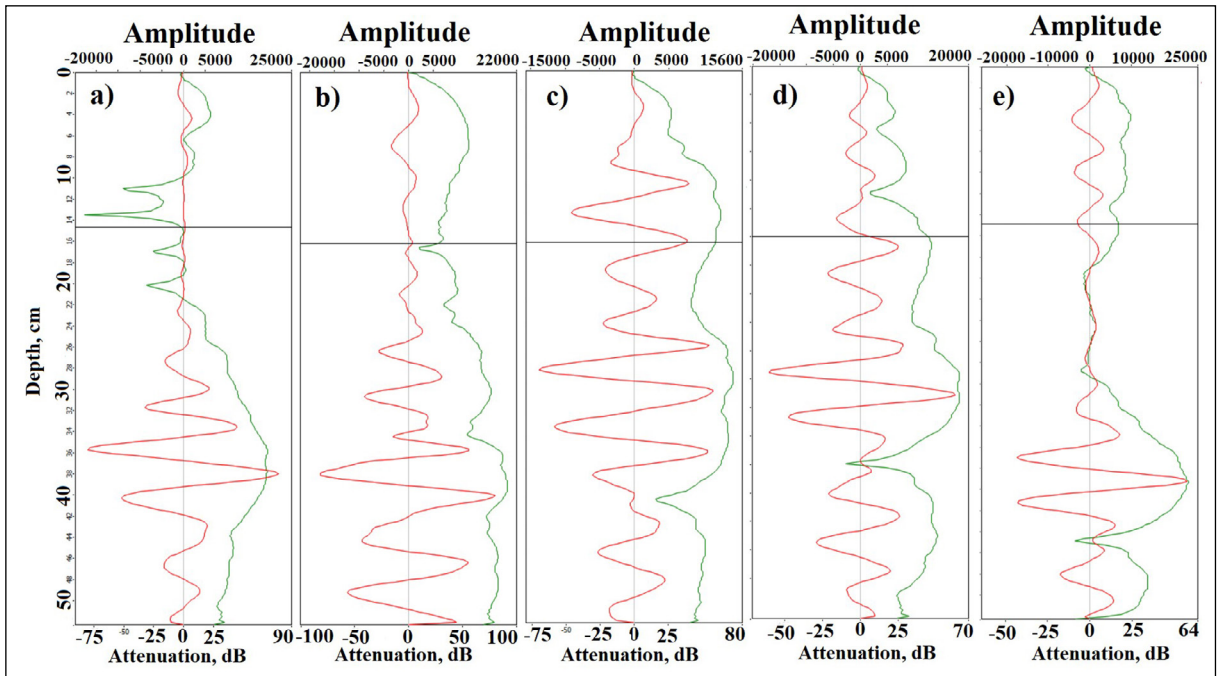


Figure 6- 1D Time-lapse vertical signal amplitude and attenuation graphs at point 50 cm. The black lines show the signal amplitudes and the red lines show the signal attenuations. a), b), c), d) and e) are the radargrams from data before contamination, one hour, 2 weeks, 4 weeks, and 26 weeks after initial contamination, respectively.

The sand was homogeneously laid down and horizontally levelled within the tank (as shown in Figure 2) to enhance uniform migration of the UEO, but as we can see from Figures 4b-e and Figures 7b-e, the migration of the UEO plume is non-uniform. Similar situation was also reported by Bano et al. (2009).

A general decrease in GPR signal amplitude in time (Figures 5 and 6) was observed below the contamination area. Similarly, a progressive decrease in signal amplitude could also be seen below the point of contamination in Figures 4c-e and Figures 7c-e. This observation was also made by several investigations such as Bertolla et al. (2014); Hagrey (2004); Bano et al. (2009); Kim et al. (2000); de Castro and Branco (2003); Bermejo et al. (1997); Sulba Rao and Chandrashekhan (2014). The unsaturated parts of the setup (Figures 4 and 7) have low reflectivity, because it is not that wet. The enhanced reflections seen directly below the point of contamination is associated with the UEO within the vadose zone. It is possible that, because of the viscous nature of the UEO, the oil migrated slowly in the vertical direction until it ended up on the water table and that during this process some

of the oil was absorbed by the sand. With the passing of time, the contaminated area within the vadose zone shows evidence of GPR signal reduction (diminished reflection) or shadow zone. Also, the distortion of the saturated part of the setup became smaller with time.

In geophysical literature, fresh contaminated sites and laboratory experiments produce enhanced GPR signal amplitude and clean GPR results, while aged contaminations are characterized by high conductivity shadow or GPR reflection reduction below the conductive zones, usually at the top of the aquifer (Atekwana and Atekwana, 2010). The findings from this experiment are an exception from the above statements in that it is relatively short term (26 weeks) but displayed characteristics of aged contamination. A study similar to the one reported here was conducted by Bertolla et al. (2014) in which they studied the migration and characterization of alkylbenzene in wet sand. They reported a slight reduction of signal amplitude within the lower vadose zone. Campbell et al. (1996) and DeRyck et al. (1993) reported that, the contamination zones that are associated with bright spots indicated floating gasoline lenses. The brightening results from an increased amplitude

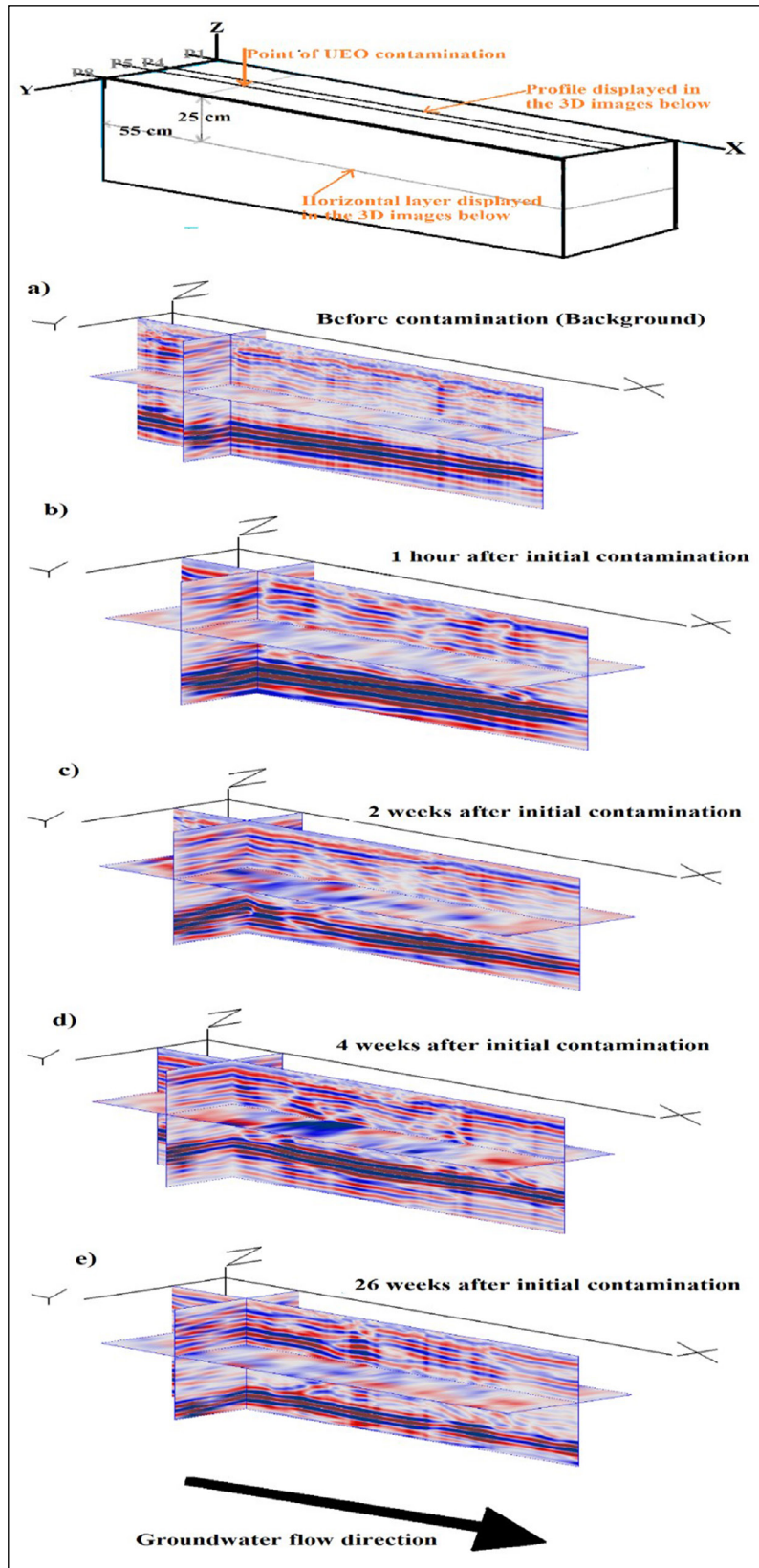


Figure 7- 3D cross sectional time-lapse of GPR radargrams showing the cross section of profile 4 and horizontal layer taken from a depth of 25cm. P1, P4, P5, P8 are the locations of profiles 1, 4, 5 and 8 respectively. a), b), c), d) and e) are the radargrams from data before contamination, one hour, 2 weeks, 4 weeks and 26 weeks after initial contamination, respectively.

(Campbell et al., 1996). Atekwana and Atekwana (2010) suggested that the replacement of water with a relatively high dielectric permittivity of ~ 80 by gasoline with a relatively low dielectric permittivity of 2 resulted in a high velocity GPR layer concomitant with bright spot as revealed in the works of Campbell et al. (1996).

We interpreted the results of the reduction of the GPR signals from the contaminated section of our setup as the results of ongoing biodegradation of the UEO contaminant. We suspected that the microbial activities might have led to the obtained results, because our setup consisted of natural sand (good environment for microbial growth), constant flow of freshwater (a source of nutrients) and a carbon source (UEO). Also, during the clean-up of the experiment tank, there was a kind of rotten smell that came out of the contaminated section of the set up. The smell was not like the oily smell of the UEO before contamination.

Our experiment was open to the atmospheric environment within the laboratory. Our experiment took place between winter (26.02.2020) and summer (19.08.2020) and that temperature variations influenced the experiment. According to Zhou and Crawford (1995), increasing temperature increases the evaporation of short-chain alkanes and other low-molecular-weight hydrocarbons. In addition, increase in temperature decreases the viscosity of hydrocarbons and their solubility in soil aqueous phase. Higher temperature cause solvent-type membrane toxicity to microorganisms (Atlas, 1975). UEO is a complex mixture of low and high (C15-C50) molecular-weight aliphatic and aromatic hydrocarbon, lubrication additives, metals, and various organic and inorganic compounds (ATSDR,1997). Increase in temperature can reduce the viscosity of the UEO and may have caused the evaporation of the low-molecular-weight hydrocarbon components of the UEO. This explanation is not satisfactory to explain the reduction in the GPR signal to nearly background levels and the rotten smell of the contaminated sand during clean-up.

It has been reported by Blume et al. (2002), that microbial activities increase in high temperature (summer) as compared to low temperature (winter). Zekri and Chaalal (2005), found out that increase

in temperature increases the microbial growth which in turn increases the degradation processes of hydrocarbons. The constant freshwater flow throughout the experiment might have provided nutrient to the contaminated zone and that might have help in acceleration of the biodegradation of the UEO. Freshwater from tap contain oxygen and water as solvent might have dissolved other nutrients such as nitrogen and phosphorus from the sand and made available to the microbes to help them grow. According to Zhou and Crawford (1995), nutrients supplied either in vapor or solution enhanced the biodegradation of hydrocarbons in soil and appropriate amount of nutrients stimulate hydrocarbon biodegradation in soil.

The possible explanation of the reduction of GPR signal with time is that; microbes might have used the organic carbon available in the UEO, the nutrients from dissolved elements in the freshwater adds mineral substrate for their growth and metabolism in the sand media. Generation of metabolic by-products such as organic acids (carbonic acids) and ionic constituents might have led to changes in the physical properties of the contaminated medium and the pore fluid chemistry which in turn changes the dielectric permittivity of the medium and increases the electrolytic and interfacial conductivity of the medium. It is well known that GPR signal reduction and depth of penetration depend on electrical conductivity and the dielectric permittivity of the medium and hence change in dielectric permittivity and increase in conductivity results changes in signal reduction. These might have led to the decrease in GPR signal with time. The finding and the interpretation of the results of this study agrees with that of several authors who carried out research in this topic. Sauck et al. (1998); Bradford (2007); Cassidy (2007), Lane et al. (2006); Atekwana and Atekwana (2010), Schilling et al. (2010), support the hypothesis with data that, increase in dissolved ionic constituents during biodegradation of LNAPL result in increases in electrical conductivity that increase GPR signal reduction with time.

4. Results

This study is the first step in understanding the GPR responses of UEO contaminated environment. The application of time-lapse GPR to UEO detection, monitoring and mapping in a sandy environment at

a laboratory experiment setting showed very good results. To the best of our knowledge, this is a first time GPR is being used to study UEO contamination with an experimental setup in laboratory. The presence of UEO plumes is identified as high amplitude signal with enhanced reflectivity, but with time the signal diminished to lower amplitudes which was interpreted as due to evaporation of some portion of the UEO in the vadose zone and due to the occurrence of UEO biodegradation.

The results presented in this paper showed that the GPR signal responses of UEO within a sandy environment change with time. Furthermore, our findings demonstrate the utility of GPR for characterizing UEO contaminated sites. The results of this study show that GPR geophysical technique can be used in addressing environmental problems associated with UEO contaminations.

Acknowledgement

The authors are grateful to the Scientific and Technical Research Council of Türkiye [TÜBİTAK (Project No: 119Y193)] and the Research Fund of Sakarya University [BAPK (Project No: 2019-7-25-37)] for supporting this study. The authors are grateful to the Sakarya University Research, Development and Application Center (SARGEM) for providing laboratory space for this experiment. We thank the personnel of the TÜPRAŞ İzmit Refinery Laboratories for the determination of physical and chemical properties of the UEO that we used in this study. We thank Prof. Dr. Halim MUTLU for editorial handling and anonymous reviewers for constructive suggestions which improved the manuscript.

Contributions to the study: Hafiz MOHAMMED NAZIFI contributed to the study conception and design and he was supervised by Prof. Dr. Levent GÜLEN. Data acquisitions were performed by Hafiz MOHAMMED NAZIFI, Ertuğrul GÜRBÜZ and Ertan PEKŞEN. Data analysis and interpretation were performed by Hafiz MOHAMMED NAZIFI and supervised by Levent GÜLEN and Ertan PEKŞEN. The first draft of the manuscript was written by Hafiz MOHAMMED NAZIFI and all authors commented on previous versions of the manuscript. All authors read and approved the final manuscript.

References

- Abioye, O. P., Agamuthu, P., Abdul Aziz, A. R. 2012. Biodegradation of used motor oil in soil using organic waste amendments. *Biotechnology Research International*, 2012, 8.
- Ameen, N. N., Klueglein, N., Appel, E., Petrovský, E., Kappler, A., Leven, C. 2014. Effect of hydrocarbon-contaminated fluctuating groundwater on magnetic properties of shallow sediments. *Studia Geophysica et Geodaetica*, 58(3), 442-460.
- Arato, A., Wehrer, M., Biró, B., Godio, A. 2014. Integration of geophysical, geochemical and microbiological data for a comprehensive small-scale characterization of an aged LNAPL-contaminated site. *Environmental Science and Pollution Research*, 21(15), 8948-8963.
- Atekwana, E. A., Atekwana, E. A. 2010. Geophysical signatures of microbial activity at hydrocarbon contaminated sites: a review. *Surveys in Geophysics*, 31(2), 247-283.
- Atekwana, E. A., Sauck, W. A., Abdel Aal, G. Z., Werkema Jr, D. D. 2002. Geophysical investigation of vadose zone conductivity anomalies at a hydrocarbon contaminated site: A implications for the assessment of intrinsic bioremediation. *Journal of Environmental & Engineering Geophysics*, 7(3), 103-110.
- Atlas, R. 1975. Effects of temperature and crude oil composition on petroleum Biodegradation. *Applied Microbiology*, 30, 396-403.
- ATSDR. 1997. Toxicological profile for used mineral-based crankcase oil.
- Azimi, R., Vaezihir, A., Lenhard, R. J., Hassanizadeh, S. M. 2020. Evaluation of LNAPL behavior in water table inter-fluctuate zone under groundwater drawdown condition. *Water*, 12(9), 2337.
- Bano, M., Loeffler, O., Girard, J. F. 2009. Ground penetrating radar imaging and time-domain modelling of the infiltration of diesel fuel in a sandbox experiment. *comptes rendus Geoscience*, 341(10-11), 846-858.
- Barber, W., Morey, R. 1994. Radar detection of thin layers of hydrocarbon contamination. In *Fifth International Conference on Ground Penetrating Radar* (pp. cp-300). European Association of Geoscientists & Engineers.
- Bermejo, J.L., Sauck, W.A., Atekwana, E.A. 1997. Geophysical discovery of a new LNAPL plume at the former Wurtsmith AFB Oscoda, MI. *Ground Water Monitoring and Remediation*, 17, 131-137.
- Bertolla, L., Porsani, J. L., Soldovieri, F., Catapano, I. 2014. GPR-4D monitoring a controlled LNAPL spill in a masonry tank at USP, Brazil. *Journal of Applied Geophysics*, 103, 237-244.

- Blume, E., Bischoff, M., Reichert, J.M., Moorman, T., Konopka, A., Turco, R.F. 2002. Surface and subsurface microbial biomass, community structure and metabolic activity as a function of soil depth and season. *Applied Soil Ecology*, 20 (3), 171–181.
- Bradford, J. H. 2007. Frequency-dependent attenuation analysis of ground-penetrating radar data. *Geophysics*, 72(3), J7-J16.
- Boumaiza, L., Chesnaux, R., Walter, J., Lenhard, R. J., Hassanizadeh, S. M., Dokou, Z., Alazaiza, M. Y. 2022. Predicting vertical LNAPL distribution in the subsurface under the fluctuating water table effect. *Groundwater Monitoring & Remediation*, 42(2), 47-58.
- Carey, A. A. 1998. The dielectric constant of lubrication oils. Computational Systems Incorporated.
- Campbell, L.D., Lucius, J.E., Maryla, D.P. 1996. Monitoring of a controlled LNAPL spill using ground penetrating radar. *The Symposium on the Application of Geophysics to Engineering and Environmental Problems*, 511–517.
- Cassidy, N. J. 2007. Evaluating LNAPL contamination using GPR signal attenuation analysis and dielectric property measurements: Practical implications for hydrological studies. *Journal of Contaminant Hydrology*, 94(1-2), 49-75.
- Charbeneau, R.J., Weaver, J.W., Lien, B.K., 1995. The Hydrocarbon spill screening model (HSSM) Volume 2: Theoretical Background and Source Codes. USEPA Publication EPA/600/R-94/039b. Washington, DC: U.S. Environmental Protection Agency.
- Daniels, D. J., Gunton, D. J., Scott, H. F. 1988. Introduction to subsurface radar, In *IEE Proceedings F, Communications, Radar and Signal Processing* 135, 4, 278-320.
- Daniels, J. J., Roberts, R., Vendl, M. 1995. Ground penetrating radar for the detection of liquid contaminants, *Journal of Applied Geophysics*, 33(1-3), 195-207.
- Davis, J.L., Annan, A.P. 1989. Ground penetrating radar for high resolution mapping of soil and rock stratigraphy. *Geophysics Prospect*, 37, 531–551.
- de Castro, D. L., Branco, R. M. G. C. 2003. 4-D ground penetrating radar monitoring of a hydrocarbon leakage site in Fortaleza (Brazil) during its remediation process: a case history. *Journal of Applied Geophysics*, 54(1-2), 127-144.
- DeRyck, S. M., Redman, J. D., Annan, A. P. 1993. Geophysical monitoring of a controlled kerosene spill, In *6th Environmental and Engineering Geophysics Society Symposium on the Application of Geophysics to Engineering and Environmental Problems*, 5-19, 209.
- Douglas, D. G., Burns, A. A., Rino, C. L., Maresca, J. W. 1992. Study to determine the feasibility of using a ground-penetrating radar for more-effective remediation of subsurface contamination, PB-92-169382/XAB).
- Ebrahimi, F., Lenhard, R. J., Nakhaei, M., Nassery, H. R. 2019. An approach to optimize the location of LNAPL recovery wells using the concept of a LNAPL specific yield, *Environmental Science and Pollution Research*, 26(28), 28714-28724.
- El-Fadel, M., Houry, R. 2001. Strategies for vehicle waste-oil management: a case study. *Resources, conservation and recycling*, 33(2), 75-91.
- Grumman Jr, D. L., Daniels, J. J. 1995. Experiments on the detection of organic contaminants in the vadose zone. *Journal of Environmental and Engineering Geophysics*, 1(A), 31-38.
- Hagrey, S. A. 2004. GPR application for mapping toluene infiltration in a heterogeneous sand model. *Journal of Environmental & Engineering Geophysics*, 9(2), 79-85.
- Kardos, S., Pietriková, A. 2016. Evaluation of motor oil characteristics and degradation factors for possibilities of continuous diagnostics, *Acta Electrotechnica et Informatica*, 16(2), 20-24.
- Kim, C., Daniels, J. J., Holt, J. J., Guy, E. D. 2000. A physical model experiment of the GPR response over gasoline, In *13th Environmental and Engineering Geophysics Society Symposium on the Application of Geophysics to Engineering and Environmental Problems*, 200, 303-310 *European Association of Geoscientists and Engineers*.
- Knight, R. 2001. Ground penetrating radar for environmental applications. *Annual Review of Earth and Planetary Sciences*, 29(1), 229-255.
- Lago, A. L., Elis, V. R., Borges, W. R., Penner, G. C. 2009. Geophysical investigation using resistivity and GPR methods: a case study of a lubricant oil waste disposal area in the city of Ribeirão Preto, São Paulo, Brazil. *Environmental Geology*, 58(2), 407-417.
- Lane, J.W., Day-Lewis, F.D., Casey, C.C. 2006. Geophysical monitoring of a field-scale biostimulation pilot project, *Ground Water*, 44(3), 430–443.
- Maceiras, R., Alfonsín, V., Morales, F. J. 2017. Recycling of waste engine oil for diesel production. *Waste management*, 60, 351-356.
- Maxwell, M., Schmock, J. 1995. Detection and mapping of an LNAPL plume using GPR: A case study, in *proceedings of the symposium on the application of geophysics to environmental and engineering problems*, *Environmental and Engineering Geophysics Society*, Englewood, Colorado, p.15-23.

- Mineo, S., Dell'Aera, F.M.L., Rizzotto, M. 2022. Evolution of LNAPL contamination plume in fractured aquifers. *Bulletin of Engineering Geology and the Environment*, 81(4), 1-14.
- Monier-Williams, M. 1995. Properties of light non aqueous phase liquids and detection using commonly applied shallow sensing geophysical techniques. *The Symposium on the Application of Geophysics to Engineering and Environmental Problems*, 1-13.
- Nazifi, H. M., Gülen, L., Gürbüz, E., Pekşen, E. 2022. Time-lapse electrical resistivity tomography (ERT) monitoring of used engine oil contamination in laboratory setting. *Journal of Applied Geophysics*, 104531.
- Newell, C. J. 1995. Light nonaqueous phase liquids. United States Environmental Protection Agency, Office of Research and Development, Office of Solid Waste and Emergency Response.
- Noln, J.J., Harris, C., Cavanaugh, P.O. 1990. *Used Oil: Disposal Options, Management Practices, and Potential Liability*, third ed. Rockville, MD: Government Institutes.
- Olhoeft, G.R. 1986. Direct detection of hydrocarbon and organic chemicals with ground penetrating radar and complex resistivity, in *Proceedings of the NWWA/API Conference on Petroleum Hydrocarbons and Organic Chemicals in Ground Water - Prevention, Detection and Restoration*, Dublin, Ohio, 284-305.
- Olhoeft, G. R. 1992. Geophysical detection of hydrocarbons and organic chemical contamination. In *5th Environmental and Engineering Geophysics Society Symposium on the Application of Geophysics to Engineering and Environmental Problems*. European Association of Geoscientists & Engineers. 587-595.
- Osweiler, G., Buck, W., Lloyd, W. 1973. Epidemiology of lead poisoning in cattle - a five-year study in Iowa. *Clinical Toxicology*, 6(3), 367-376.
- Propst, T.L., Lochmiller, R.L., Qualis, C.W., McBee, K. Jr. 1999. In situ (mesocosm) assessment of immunotoxicity risks to small mammals inhabiting petrochemical waste sites. *Chemosphere*, 38, 1049-1067.
- Redman, J.D., DeRyck, S.M., Annan, A.P. 1994. Detection of LNAPL pools with GPR: theoretical modelling and surveys of a controlled spill, in *Proceedings of the International Conference on Ground-Penetrating Radar*, Kitchener, Ontario, Canada, 1283-1294.
- Sas, B. 1989. Secondary copper deficiency in cattle caused by molybdenum contamination of fodder: A case history. *Veterinary and Human Toxicology*, 31(1), 29-33.
- Sauck, W.A., Atekwana, E.A., Nash, M.S. 1998. High conductivities associated with an LNAPL plume imaged by integrated geophysical techniques. *Journal of Environmental and Engineering Geophysics*, 2, 203-212.
- Schillig, P.C., Tsofiias, G.P., Roberts, J.A., Patterson, E.M., Devlin, J.F. 2010. Ground-penetrating radar observations of enhanced biological activity in a sandbox reactor, *Journal of Geophysical Research*, 115, G00G10.
- Sulba Rao Ch., Chandrashekhar, V. 2014. Detecting oil contamination by ground penetrating radar around an oil storage facility in Dhanbad, Jharkhand, India. *Journal of Indian Geophysical Union*, 18(4), 448-454.
- Tomlinson, D. W., Rivett, M. O., Wealthall, G. P., Sweeney, R. E. 2017. Understanding complex LNAPL sites: Illustrated handbook of LNAPL transport and fate in the subsurface. *Journal of Environmental Management*, 204, 748-756.
- US Department of Health and Human Services, Public Health Service PHS, Agency for Toxic Substances and Disease Registry
- USEPA (United States Environmental Protection Agency) 1993. *Use of Airborne, Surface, and Borehole Geophysical Techniques at Contaminated Sites*.
- USEPA (United States Environmental Protection Agency) 1996. *How to Effectively Recover Free Product at Leaking Underground Storage Tank Sites: A Guide for State Regulators*.
- USEPA (United States Environmental Protection Agency) 2000. *Innovations in Site Characterization: Geophysical Investigation at Hazardous Waste Sites*.
- Werkema Jr, D. D., Atekwana, E. A., Endres, A. L., Sauck, W. A., Cassidy, D. P. 2003. Investigating the geoelectrical response of hydrocarbon contamination undergoing biodegradation. *Geophysical Research Letters*, 30(12).
- Zekri, A. Y., Chaalal, O. 2005. Effect of temperature on biodegradation of crude oil. *Energy Sources*, 27(1-2), 233-244.
- Zhou, E., Crawford, R. L. 1995. Effects of oxygen, nitrogen, and temperature on gasoline biodegradation in soil. *Biodegradation*, 6(2), 127-140.